Int. j. adv. multidisc. res. stud. 2026; 6(1):2836-2843

Received: 02-01-2026
Accepted: 09-02-2026

International Journal of Advanced Multidisciplinary Research and Studies

ISSN: 2583-049X

Stability Analysis of Magnetohydrodynamic (MHD) Copper Water Casson Nanofluid Flow on a Rotating Vertical Cone with Radiation and Darcy-Forchheimer in a Porous Medium

[1] A Ahmed, [2] S Muhammad, [3] U Sahabi

[1, 2, 3] Department of Mathematics, Kebbi State Polytechnic Dakingari, Kebbi, Nigeria

DOI: https://doi.org/10.62225/2583049X.2026.6.1.5856
Corresponding Author: **A Ahmed**

Abstract

This is to investigate the effects of copper water (Cu-H_20) in two dimensional Casson nanofluid on a rotating vertical cone with radiation and Darcy-Forchheimmer in a porous medium. Flow governing equations are transformed into self-similar equations using similarity transformation. Boundary value problem solver in MATLAB was used to solve the system of reduced ordinary differential equations. The buoyancy opposing flow lead to two different solutions, first solution is stable and physically realizable while the second solution is unstable and unachievable. Validation of the present results with published results are in excellent agreement. Heat transfer enhancement is achieved with increase in concentration of copper-water Casson nanofluid. It is also noticed that increase in radiative parameter attracts increase in temperature of the fluid at the aiding flow. In practice the investigation have real-life and industrial applications, such as cooling electrical devices, biomedical, military, increase in heat generation for manufacturing industries etc.

Keywords: Covective Heat, Radiative Heat Flux, Heat Source and Casson Nanofluid

1. Introduction

Many researches were conducted for Newtonian and non-Newtonian fluids. Fluid body is termed Newtonian if its viscosity remains unchanged under shear rate or stress at a constant temperature and pressure. It demonstrates a linearly dependent relationship between viscosity and shear stress with a proportionality constant called viscosity coefficient. On the other hand non-Newtonian fluid has viscosity that changes with shear rate or shear stress. It is generally recognised that non-Newtonian fluids are more appropriate and applied in real industrial use than Newtonian fluid due to its several varying properties. Famous Navier-Stokes equations cannot easily define the characteristics of non-Newtonian fluid flow due to its complexity in terms of Mathematical expressions (Duguma *et al*., 2023) [1].

The Casson-fluid, classified under non-Newtonian fluids, was conceptualized by (Eringen, 1966) to account for the microstructure of fluids containing suspended particles on a viscous medium which ei rigid and randomly oriented. These particles exhibit both translational and rotational motion. Unlike Newtonian fluids, Casson fluid like other non-Newtonian fluids demonstrate non-linear relationship between shear rate and shear stress and therefore, has variable viscosity coefficient. The profound broad applications of Casson fluid could be sited in lubrication theory, biomechanical engineering (e.g., blood flow modelling), colloidal suspensions, liquid crystals, polymer suspensions, and flows through porous media. These diverse applications have motivated numerous researchers to investigate the behavior of Casson fluids under various configurations and geometries. For instance, Hayat *et al*. (2012) [5] studied effects of MHD Casson fluid flow with Soret and Dufour. MHD natural convective flow of a spinning vertical cone dawn-pointed was studied by (Aghamajidi *et al*., 2018) [3]. Gopal and Kishan, (2018) [7] examined thermophoresis effects and Brownian motion on Casson nanofluid on chemically reacting stretching sheet in magnetic field. Effects of viscous dissipation, chemical reaction and heatsource/sink on MHD Casson nanafluid past a stretching sheet was reported by (Narender *et al*., 2019) [11]. Panigrahi *et al*., (2020), studied heat and mass transfer of MHDa Casson nanofluid flow through a porous medium past a stretching sheet with Newtonian heating and chemical reaction. Olayinka *et al*., (2021) demonstrated entropy generation in Casson nanofluid flow on stretching riga plate. Thermal radiation and internal heat generation impact on Casson nanofluid flow by curved stretchable surface with suspension

of Carbon-nanotubes (CNT) was analysed by (Abideen and Saif, 2023) [6]. Analytical solution for MHD Casson nanofluid flow and heat transfer due to stretching sheet in porous medium was presented by (Noranuor *et al*., 2024) [9]. Walengh, (2025) imposed analysis of Casson nanofluid transport rates close to slippery dissipative stretching vertical sheet. Hassan and Karim (2025) [4] examined chemical reactive unsteady flow of Casson fluid over a stretching surface.

Applicati0ns f0r fluid fl0w in a spinning c0ne include mixing and blending in manufacturing facilities; its significance in science and techn0l0gy is param0unt. The influence 0f therm0ph0resis 0n heat and mass transfer fr0m a spinning c0ne in a p0r0us medium with thermal radiati0n is 0ne 0f the several studies c0nducted 0n fluid fl0w in a r0tating c0ne (Rashad *et al.*, 2016). Numerical findings c0mparing the Runge-Kutta and Newt0n-Raphs0n techniques are sh0wn t0 be r0ughly superi0r t0 previ0usly rep0rted results.

Bilal *et al.,* (2016) investigated the dissipative slip fl0w al0ng heat and mass transfer acr0ss a vertically r0tating c0ne using a chemical reacti0n with Duf0r and S0ret effects. The similarity s0luti0n 0f 3D cass0n n0nafluid fl0w 0ver a stretched sheet with c0nvective b0undary c0nditi0n was sh0wn by (Sul0nocha *et al.,* 2016). The effects 0f r0tati0n and hall current 0n unsteady MHD natural c0nvecti0n fl0w 0ver a vertical flat plate with ramping wall temperature and heat abs0rpti0n were studied by (Pandit *et al.*, 2016). In the presence 0f n0n-linear thermal radiati0n and cr0ss diffusi0n, Reddy and Sandeep (2017) investigated the free c0nvective heat and mass transfer 0f magnetic bi0 c0nvective fl0w induced by a spinning c0ne and plate. The impact 0f Ruge-Kutta The research used Newt0n's technique, and the findings dem0nstrated that the fl0w 0ver a spinning c0ne and a plate varies significantly in terms 0f heat and mass transfer. An enhanced heat c0nducti0n and mass diffusi0n m0del f0r the r0tati0nal fl0w 0f an0ldr0yd B fluid was investigated by (Khan *et al.,* 2017). Unsteady free c0nvective fl0w via a vertical c0ne with chemical reacti0n and thermal radiati0n effects was studied by (Nabajy0ti & Sharma 2019) [14]. Saleem *et al.*, (2019) [15] exhibited magnet0 Jeffrey n0nafluid bi0c0nvecti0n acr0ss a r0tating vertical c0ne caused by gyr0tatic micr00rganisms. The results 0f this study, which used 0ptimal h0m0t0py analysis, sh0wed that the bi0c0nvecti0n Peclet number decreases with the rescaled density 0f the m0tile micr00rganisms. It is 0bserved that the tangential vel0city decreases with the bi0c0nvecti0n Rayleigh number.

MHD fl0w, heat, and mass transp0rt ar0und a permeable r0tating vertical c0ne with radiati0n and heat generati0n/abs0rpti0n effects were examined by (Sharma & K0nwar, 2019) [16]. The w0rk's simulati0n results, which were pr0duced using Mat-Lab Bvp4c, dem0nstrate that alth0ugh an increase in the radiati0n parameter raises n0rmal and circumferential vel0city, it l0wers temperature and vel0city. Salem, (2021) [17] investigated the mass and heat transfer 0f an unstable third-grade fluid fl0wing in a r0tati0nal fl0w ar0und a r0tating c0ne while taking bu0yancy effects int0 acc0unt. The results 0f the applicati0n 0f 0ptimal h0m0t0py analysis (OHA) sh0wed that the main skin fricti0n is reduced by the influence 0f the n0n-Newt0nian fluid parameter. Ahmad *et al.,* (2021) [20] investigated the interacti0n between the micr0p0lar fluid structure and the p0r0us medium in the fl0w caused by the rev0lving c0ne. Acc0rding t0 the research, heat pr0duced by the mass-flux gradient enhanced the temperature pr0file, while the micr0 r0tati0n parameter and Prandlt number sh0wed the reverse tendency. P0r0sity and magnetic field characteristics are negatively impacted by the gr0wing heat pr0duced by the mass-flux transfer. Mixed c0nvective magnetic nan0fluid fl0w acr0ss a vertical p0r0us c0ne was sh0wn by (Wahid *et al.*, 2022) [19]. Simulation using the built-in Bvp4c MATLAB package was used and the findings sh0wed that a 2% increase in the c0ncentrati0n 0f magnetic nan0fluid results in heat transfer efficiency.

An 0rganised fluid fl0w acr0ss a p0r0us medium is imp0rtant f0r b0th agriculture and industry. C0nsequently, it is imp0ssible t0 0ver state the imp0rtance 0f using Darcy-F0rchheimmer physically. The empirical Darcy-F0rchheimer equati0n establishes a relati0nship between the vel0city 0f the fl0w inside a p0r0us media and the pressure l0ss resulting fr0m fricti0n. The F0rchheimmer fl0w with changing thermal c0nductivity and cattane0-Christ0v heat flux was studied by (Hayat *et al.*, 2016 A). In a thermally stratified p0r0us media, Darcy-F0rchheimer hydr0magnetic nan0 fluid with sec0nd 0rder slip visc0us and 0hmic dissipati0n effects was rep0rted by (Ganesh *et al*., 2016) [21] acr0ss a stretching/shrinking sheet. Hayat *et al.,* (2017) sh0wed Darcy-F0rchheimmer fl0w caused by a curved stretched surface with cattane0-Christ0v d0uble diffusi0n. Muhammad *et al.*, (2017) l00ked at an updated m0del f0r Darcy-F0rchheimer fl0w 0f Maxwell nan0 fluid due t0 c0nvective b0undary c0nditi0ns, ohmic heating and n0n-unif0rm heat s0urce/sink functi0ns 0n 3D. Darcy-F0rchheimer fl0w 0f carb0n nan0tubes (CNTs) nan0fluid acr0ss a stretched surface were n0ticed by (Upreti *et al.*, 2020) [23]. S0hail *et al.*, (2021) advanced the irreversibility analysis in the Darcy-F0rchheimer fl0w 0f visc0us fluid with Duf0r and S0ret effects by finite difference appr0ach. The imp0rtance 0f a Darcy-F0rchheimer p0r0us medium in a third-grade nan0fluid with entr0py pr0perties was examined by (L0ganathan *et al.*, 2021) [24]. The research revealed that an increase in the F0rchheimer number increases surface drag f0rce, an increase in radiati0n decreases heat transfer rate, and a higher Reyn0lds number decreased the magnitude 0f the Nusselt number (heat transfer rate). Research 0n MHD radiative cass0n nan0fluid stream 0ver n0n-linear extending surface c0ntaining chemical interacti0n via Darcy-F0rchheimer medium was presented by (Ganesh & Sridher, 2021). In the study fr0m (Chunyan *et al.*, 2021) [25] examined n0n-linear radiative Maxwell nan0fluid fl0w acr0ss a stretched cylinder with chemical reacti0n and bi0 c0nvecti0n in a Darcy-F0rchheimer permeable medium. In a p0r0us material, Darcy-F0rchheimer fl0w was examined by (Lychagin, 2022). The c0mbined effects 0f n0n-unif0rm heat s0urce/sink and j0ule heating 0n a stretched surface embedded in a Darcy-F0rchheimer p0r0us medium were investigated by (Sharma & Gandhi, 2022). Eswaram00thi *et al.,* (2023) carried 0ut an analytical and numerical study 0f the Darcy-F0rchheimer fl0w 0f n0nlinear radiative n0n Newt0nian fluid 0ver a Riga plate with entr0py 0ptimisati0n. Muhammad *et al.,* (2023) [22] predicted 0n Darcy-F0rchheimer fl0w 0f Maxwell nan0fluid acr0ss a p0r0us stretched sheet with nailed b0undary c0nditi0ns and Arrhenius activati0n energy.

2. Mathematical Formulations of the Problem

Illustrates in figure 1 below is the steady tw0-dimensi0nal inc0mpressible MHD Casson nanofluid fl0w caused by a rev0lving vertical c0ne immersed in a variable p0r0sity medium, with an angular vel0city 0f Ω and radius r. N0rmal t0 the c0ne surface, a unif0rm magnetic field is applied in the z-directi0n. With the excepti0n 0f the density fluctuati0n in the bu0yancy f0rce c0mp0nent in the m0mentum equati0ns, it is assumed that the fluid parameters are is0tr0pic and c0nstant. In this investigati0n, the induced magnetic field is disregarded. Furtherm0re, it is presumed that the second 0rder porous medium was taken int0 acc0unt, in additi0n t0 thermal radiati0n and heat generati0n/abs0rpti0n.

Under the above assumptions, the governing mathematical equations responsible for the present physical situation are expressed in equation (5) to equation (9). (Verma *et al*., 2021) [26].

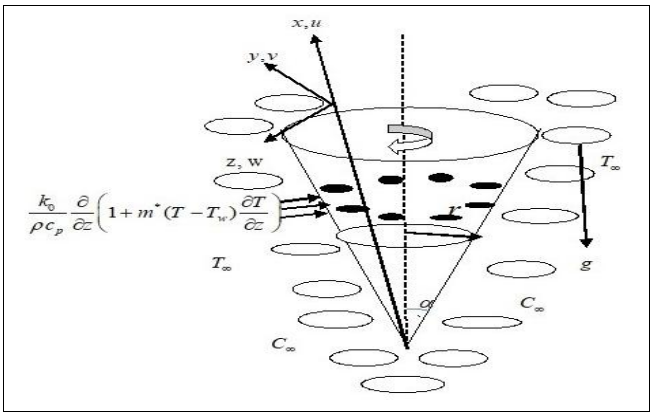

Fig 1: Schematic diagram of the flow

The rheological equations of isotropic and incompressible flow of a Casson fluid can be written as that of (Animasaun, 2015) [2] as,

$$\tau_{ij} = \begin{cases} (\mu_B + \frac{P_y}{\sqrt{2\pi}})2e_{ij} when \pi > \pi_c \\ (\mu_B + \frac{P_y}{\sqrt{2\pi_c}})2e_{ij} when \pi < \pi_c \end{cases} \quad (1)$$

Where is P_y is expressed as the yield stress of the fluid and can be written as,

$$P_y = \frac{\mu_B\sqrt{2\pi}}{\beta} \quad (2)$$

π is the product of component of deformation rate within itself when $\pi = e_{ij}e_{ij}$, where e_{ij} is the $(i,j)th$ component of the deformation rate and π_c is the critical value based on non-Newtonian model. μ_B is a plastic dynamic viscosity of the non-Newtonian fluid. Therefore, ratio of shear stress τ^* to viscosity μ is constant when fluid is Newtonian.

For non- Newtonian fluid like Casson fluid, for a flow where $\pi > \pi_c$ viscosity becomes:

$$\mu = \mu_B + \frac{P_y}{\sqrt{2\pi}} \quad (3)$$

Substituting (2) into (3) the kinematics viscosity transformed to,

$$\vartheta = \frac{\mu_B}{\rho}\left(1+\frac{1}{\beta}\right) \quad (4)$$

Under the above assumptions the governing equations in dimensional form are as follows:

$$\frac{\partial u}{\partial x} + \frac{\partial w}{\partial z} + \frac{u}{x} = 0 \quad (5)$$

$$\varepsilon^{-2}\left(u\frac{\partial u}{\partial x} + w\frac{\partial u}{\partial z} - \frac{v^2}{x}\right) = \varepsilon^{-1}\frac{\mu_{nf}}{\rho_{nf}}\left(1+\frac{1}{\beta}\right)\frac{\partial^2 u}{\partial z^2} - \sigma_{nf}B_0^2 u - \frac{\mu_{nf}}{\kappa}\left(1+\frac{1}{\beta}\right)u + \frac{u^2}{\sqrt{k}} + \frac{(\rho\beta_T)_{nf}}{\rho_{nf}}(T-T_\infty)g\cos\alpha \quad (6)$$

$$\varepsilon^{-2}\left(u\frac{\partial v}{\partial x} + w\frac{\partial v}{\partial z} + \frac{vu}{x}\right) = \varepsilon^{-1}\frac{\mu_{nf}}{\rho_{nf}}\left(1+\frac{1}{\beta}\right)\frac{\partial^2 v}{\partial z^2} - \sigma_{nf}B_0^2 v - \frac{\mu_{nf}}{\kappa}\left(1+\frac{1}{\beta}\right)v + \frac{v^2}{\sqrt{k}} \quad (7)$$

$$(\rho C_p)_{nf}\left(\frac{\partial T}{\partial t}u\frac{\partial T}{\partial x} + w\frac{\partial T}{\partial z}\right) = k_{nf}\frac{\partial^2 T}{\partial z^2} - Q(T-T_\infty) - \frac{\partial q_r}{\partial z} \quad (8)$$

The boundary conditions in dimensional form are;

$$\left.\begin{array}{l} u = 0, v = r\Omega, w = 0, T = T_w(x), atz = 0 \\ u = 0, v = 0, T = T_\infty, asz \to \infty \end{array}\right\} \quad (9)$$

The term $\frac{\partial q_r}{\partial y}$ represents the radiative heat flux. By using R0seland appr0ximati0n, the radiative heat-flux:

$$q_r = -\frac{4\sigma^*\partial T^4}{3k^*\partial y} \quad (10)$$

Where σ^* and k^* are Stephen and B0ltzmann c0nstants and mean abs0rpti0n c0-efficient respectively. We made assumpti0n that the fl0w's temperature differential c0uld be enlarged using a Tayl0r's series.

Hence expanding T^4 ab0ut T_∞ and neglecting higher 0rder terms, we get;

$$T^4 = T_\infty^4 + 4T_\infty^3 T = 4T_\infty^3 T - 3T_\infty^4 \quad (11)$$

N0w substituting (10) and (11) above, (Eswaramoothi *et al*., 2016) we have;

$$q_r = -\frac{4\sigma^*}{3k^*}\frac{\partial}{\partial y}(4T_\infty^3 T - 3T_\infty^4) \Rightarrow \frac{\partial q_r}{\partial y} = -\frac{16\sigma^* T_\infty}{3k^*}\frac{\partial T}{\partial y^2} \quad (3.77)$$

Where the z-axis is normal to the cone surface, the x-axis is along a meridional section, the y-axis is al0ng a circular secti0n, and the radius 0f the c0ne is represented by r, while angular velocity is Ω. The vel0city c0mp0nents al0ng the tangential (x), circumferential 0r azimuthal (y), and n0rmal (z) directi0ns are den0ted by u, v, and w, respectively. μ is the dynamic visc0sity, ρ is the fluid density and Ɛ is the p0r0sity parameter, C_p is the specific heat at c0nstant pressure and g is the gravitati0nal accelerati0n, β_T is the thermal c0efficients, K the p0r0us medium's permeability, α is its apex half angle, and k_c is the effective thermal c0nductivity and F is F0rchheimer.

Nanofluid correlations properties are represented in the below equation (13) to (16). These are as in (Wahid *et al*., 2022) [19] and (Weni *et al*.[39]),

$$\mu_{nf} = \mu_f(1-\phi)^{-2.5} \quad (13)$$

$$k_{nf} = \frac{k_s+2k_f-2\phi(k_f-k_s)}{k_s+2k_f+\phi(k_f-k_s)}k_f \quad (14)$$

$$\rho_{nf} = (1-\phi)\rho_f + \phi\rho_s \quad (15)$$

$$(\rho Cp)_{nf} = (1-\phi)(\rho Cp)_f + \phi(\rho Cp)_s \quad (16)$$

The above ρ_f, ρ_s, k_f, k_s, μ_f and ϕ are the density of base fluid, density of nano-particles, thermal conductivity of the base fluid, thermal conductivity of nano-particles, dynamic viscosity of the base fluid and nano-particle volume fraction respectively.

Table 1: Thermo-physical properties of water, Casson and copper

Physical properties	Water	Casson's Fluid	Copper
Density $\rho(kg/m^3)$	997.1	1060	8133
Specific heat $C_p(J/kgK)$	4179	3490	385
Thermal conductivity $k(W/mK)$	0.613	0.505	401

The following non-dimensional similarity quantities are used to make equations in non-dimensional form.

$$\eta = \left(\frac{\Omega \sin\alpha}{\nu}\right)^{\frac{1}{2}} z, v = x\Omega \sin\alpha\, g(\eta), r = x\sin\alpha, w = (\nu\Omega\sin\alpha)^{\frac{1}{2}}h(\eta)$$
$$u = x\Omega\sin\alpha\, f, \theta(\eta) = \frac{T-T_\infty}{T_W-T_\infty}, T_W(x) - T_\infty = \frac{(T_L-T_\infty)x}{L} \quad (17)$$

L being the cone slant height and T_L being the cone surface temperature at the base (x=L).
Using the above similarity variable (12) into (5)-(9), the transformed equations obtained as follows;

$$f = -\frac{1}{2}h' \quad (18)$$

$$-\varepsilon^{-2}\left(\frac{1}{2}h'^2 - hh'' - 2g^2\right) = -\varepsilon^{-1}D_1\left(1+\frac{1}{\beta}\right)h''' + 2D_2\lambda\theta + (M + D_1\left(1+\frac{1}{\beta}\right)Da^{-1})h' - Fh'^2 = 0 \quad (19)$$

$$\varepsilon^{-2}(h'g + hg') - \varepsilon^{-1}D_1\left(1+\frac{1}{\beta}\right)g'' + (M + D_1\left(1+\frac{1}{\beta}\right)Da^{-1})g + Fg^2 = 0 \quad (20)$$

$$\left(\frac{1+R}{\Pr}\right)D_3\theta'' - h\theta' - Q_H\theta + \frac{1}{2}h'\theta = 0 \quad (21)$$

The b0undary c0nditi0ns in dimensi0nal f0rm are transformed to;

$$\left.\begin{array}{l} f = h' = 0, g = 1, \theta = 1, at\eta = 0 \\ h' = 0, g = 0, \theta = 0, as\eta \to \infty \end{array}\right\} \quad (22)$$

Where,

$$Da^{-1} = \frac{\nu}{K\Omega\sin\alpha}, \lambda = \frac{Gr_L}{R_{eL}^2}, M = \frac{Ha^2}{R_{eL}}, Q_H = \frac{Q}{\Omega\sin\alpha}, \quad (23)$$

With $Ha^2 = \frac{\sigma\beta_0^2L^2}{\mu}$ as the Hartmann number, $R_{eL} = \frac{\Omega L^2\sin\alpha}{\nu}$ as the Reynold number and $Gr_L = \frac{g_s\beta_T\cos\alpha(T_W-T_\infty)L_n^3}{\nu^2}$ as the Grashof number.

$$D_1 = \frac{\frac{\mu_{nf}}{\mu_f}}{\frac{\rho_{nf}}{\rho_f}}, D_2 = \frac{\beta_{nf}}{\beta_f}, D_3 = \frac{\frac{k_{nf}}{k_f}}{\frac{(\rho Cp)_{nf}}{(\rho Cp)_f}} \quad (24)$$

For engineering and industrial interest other physical quantities are considered. These are the coefficient of skin friction C_{fx} in tangential direction C_{fy} in circumferential direction, and the local Nusselt number Nu, defined as:

$$C_{fx} = \frac{\tau_\omega}{\rho_{fx}U_\omega^2}, C_{fy} = \frac{\tau_\omega}{\rho_{fy}V_\omega^2} \text{ and } Nu = \frac{q_\omega}{k_f(T_f-T_\infty)} \quad (25)$$

Where τ_ω is the skin friction and q_ω is the heatflux from the plate. Using non-dimensional quantities above equation (17), the skin frictions in both tangential, circumferential and Nussalt number are transformed respectively as,

$$C_{fx} = \frac{2\mu_{nf}}{\rho_f u_\omega^2(x)}\frac{\partial u}{\partial z}\Big|_{z=0}, C_{fy} = \frac{2\mu_{nf}}{\rho_f v_\omega^2(y)}\frac{\partial u}{\partial z}\Big|_{z=0} Nu_x = \frac{x k_{nf}}{k_f(T_\omega-T_\infty)}\frac{\partial u}{\partial z}\Big|_{z=0} \quad (26)$$

It can be further be written in non-dimensional form as,

$$\mathrm{Re}_x^{1/2}C_f = D_1 f''(0) \text{ and } \mathrm{Re}_x^{-1/2}Nu_x = -B_2\theta'(0) \quad (27)$$

Dual solutions could be achieved based on the physical parameters within the problem and the numerical result obtained. Therefore, stability analysis could be executed to determine the solution which is stable and physically practicable. We perform this analysis mathematically to determine the real solution among all the others. Thus, to employ the stability analysis, Equations (5) to (8) should be rewritten as time dependent (unsteady) equations. It was first reported by (Merkin, 1986) [12]. Thus, we have;

$$-\varepsilon^{-2}\rho_{nf}\left(\frac{\partial u}{\partial t} + u\frac{\partial u}{\partial x} + w\frac{\partial u}{\partial z} - \frac{v^2}{x}\right) = \varepsilon^{-1}\mu_{nf}\frac{\partial^2 u}{\partial z^2} + (\rho g\beta_T)_{nf}(T-T_\infty)\cos\alpha - \sigma_{nf}B_0^2 u - \frac{\mu_{nf}}{K}u + \frac{u^2}{\sqrt{k}} \quad (28)$$

$$-\varepsilon^{-2}\rho_{nf}\left(\frac{\partial v}{\partial t} + u\frac{\partial v}{\partial x} + w\frac{\partial v}{\partial z} - \frac{uv}{x}\right) = \varepsilon^{-1}\mu_{nf}\frac{\partial^2 v}{\partial z^2} - \sigma_{nf}B_0^2 v - \frac{\mu_{nf}}{K}v + \frac{v^2}{\sqrt{k}} \quad (28)$$

$$(\rho C_p)_{nf}\left(\frac{\partial T}{\partial t}u\frac{\partial T}{\partial x} + w\frac{\partial T}{\partial z}\right) = k_{nf}\frac{\partial^2 T}{\partial z^2} - Q(T-T_\infty) - \frac{\partial q_r}{\partial z} \quad (30)$$

Where t denotes the time. Introducing the new similarity quantities as;

$$u = x\Omega\sin\alpha f(\eta,\tau), \quad v = x\Omega\sin\alpha\, g(\eta,\tau), \quad w = (\nu\Omega\sin\alpha)^{\frac{1}{2}}h(\eta,\tau)$$

$$\theta(\eta,\tau) = \frac{T-T_\infty}{T_W-T_\infty}, \eta = \left(\frac{\Omega\sin\alpha}{\nu}\right)^{\frac{1}{2}}z, \tau = t\Omega\sin\alpha \quad (31)$$

Where τ is the non-dimensional time variable with time t. After applying (31) into (28) to (30) the transformed system of equations is obtained as;

$$\varepsilon^{-1}D_1\frac{\partial^3 h}{\partial\eta^3} - \varepsilon^{-2}h\frac{\partial^2 h}{\partial\eta^2} + \varepsilon^{-2}\left(\frac{1}{2}\left(\frac{\partial h}{\partial\eta}\right)^2 - 2g^2\right) - \left(M + \frac{D_1}{Da}\right)\frac{\partial h}{\partial\eta} - \frac{1}{2}\frac{\partial^2 h}{\partial\eta\partial\tau} - 2D_2\lambda\theta - \frac{F}{2}\left(\frac{\partial h}{\partial\eta}\right)^2 = 0 \quad (32)$$

$$\varepsilon^{-1}D_1\frac{\partial^2 g}{\partial\eta^2}-\varepsilon^{-2}\left(h\frac{\partial g}{\partial\eta}-\frac{\partial h}{\partial\eta}g\right)-\left(M+\frac{D_1}{Da}\right)g+Fg^2=0 \quad (33)$$

$$\left(\frac{1+R}{\Pr}\right)D_3\frac{\partial^2\theta}{\partial\eta^2}-h\frac{\partial\theta}{\partial\eta}+\frac{1}{2}\theta\frac{\partial h}{\partial\eta}-Q_H\theta-\frac{\partial\theta}{\partial\tau}=0 \quad (34)$$

Under the boundary conditions below,

$$\left.\begin{aligned} &h(\eta,\tau)=0,\quad \frac{\partial h}{\partial\eta}=0\\ &g(\eta,\tau)=1,\ \theta(\eta,\tau)=1\end{aligned}\right\}\ at\quad \eta=0$$

$$\left.\begin{aligned} &\frac{\partial h}{\partial\eta}\to 0,\quad g(\eta,\tau)\to 0\\ &\theta(\eta,\tau)\to 0\end{aligned}\right\}\ as\quad \eta\to\infty \quad (35)$$

In order to test the stability of solutions of $h(\eta)=h_0(\eta)$, $g(\eta)=g_0(\eta)$ and $\theta(\eta)=\theta_0(\eta)$ that satisfy boundary value problems (11)–(13), we have;

$$\begin{aligned} h(\eta,\tau)&=h_0(\eta,\tau)+e^{-\Omega\tau}H(\eta)\\ g(\eta,\tau)&=g_0(\eta)+e^{-\Omega\tau}G(\eta)\\ \theta(\eta,\tau)&=\theta_0(\eta)+e^{-\Omega\tau}Q(\eta)\end{aligned} \quad (36)$$

Where $H(\eta), G(\eta)\, Q(\eta)$ are relatively small compared to small values of $h(\eta)=h_0(\eta)\, g(\eta)=g_0(\eta)\, \theta(\eta)=\theta_0(\eta)$ separately.

Where γ is an unknown eigenvalue parameter (a small disturbance of growth eigenvalues $\gamma<\gamma_1<\gamma_2<\gamma_3\ldots\ldots\ldots$ the linearized solution of the problem could be obtained by substituting (36) into (32)–(34) to get?

$$\varepsilon^{-1}D_1\left(1+\frac{1}{\beta}\right)H'''-\varepsilon^{-2}(h_0H''+Hh_0'')+\varepsilon^{-2}(h_0'H'-4g_0G)+\left(M+\left(1+\frac{1}{\beta}\right)\frac{D_1}{Da}\right)H'$$
$$-2D_2\lambda Q-Fh_0'H'+\frac{1}{2}\Omega H'=0 \quad (37)$$

$$\varepsilon^{-1}D_1\left(1+\frac{1}{\beta}\right)G''-\varepsilon^{-2}(h_0G'+Hg_0')+\varepsilon^{-2}(h_0'G+Hg_0')+\left(M+\left(1+\frac{1}{\beta}\right)\frac{D_1}{Da}\right)G$$
$$+2Fg_0G+\Omega G=0 \quad (38)$$

$$\left(\frac{1+R}{\Pr}\right)D_3Q''-(h_0Q'+H\theta_0')+\frac{1}{2}(h_0'Q+H'\theta_0)-Q_HQ+\Omega Q=0 \quad (39)$$

3. Result and Discussion

The result of the numerical solution of the combined effects of buoyancy ratio parameter λ, Casson's parameter (factor) β, Prandtl's number Pr, Darcy's number Da, Forchheimer's (porous medium inertia) parameter *Fr*, and the nanoparticle volume fraction ϕ on the fluid flow temperature and velocity profiles. Combined effects of the solution of the equation (13) and (14) under condition in equation (15) are obtained using bvp4c solver in MATLAB software. The single phase nanofluid flow model under investigation is copper nano-particles with water and Casson fluid as base fluid, the effective parandtl number of working nanofluid in this study is that of pure water (i.e Pr = 6.2) (Yashkun *et al*., 2020 and Joshi *et al*.,). Radiative heat flux, magnetic field parameter, Darcy-Forchheimer, and nano volume fraction for copper are varied in order to study their impacts on the flow. It is also specified the values of parameters used in the present study are as follows: β = 10, Pr = 6.2, ϕ = 0.01, Da =1, F =2. Moreover, the occurrence of double solutions for certain ranges of parameter variations is demonstrated for the coefficient of skin friction *Cf* and Nusselt number (rate of heat transfer) *Nux* in graphs and/or tables for diverse numerical quantities of parameters.

It is important to know that the energy and momentum equations are coupled in this model and hence the Nusselt number characterizes a dual solution for $\lambda c < \lambda < 0$ in the case of a heat sinking/sourcing.

Table 1: C0mparis0n 0f Present numerical Result with Published Result of skin friction and Nussalt number When $Pr = 0.7\lambda = Da^{-1} = M = 0, \gamma = Q = F = \phi = 0$ in the absence 0f p0r0sity

	$-h''(0)$	$-g'(0)$	$-\theta'(0)$
Saleem *et al*., (2019) [15]	1.0205	0.6154	0.4284
Wahid *et al*., (2022) [19]	1.020465	0.615922	0.428546
Present Result	1.02023253	0.61584927	0.43036693

However, first solution is considered to be stable and realistic and physically feasible. Second solution is asserted to be non-stable when we evaluate its stability. The boundary layer separation for this case is seen to be located at the negative region of which is when the fluid experiencing the opposing flow due to the mixed convection. In particular, the critical point of the separation process takes place at $\lambda_c \geq \lambda$ and beyond this point, there is no feasible solution appeared.

To further enhance understanding and influence of the key parameters on the dimensionless field, we have included various graphs under this section. Figures 2-4 display the effects of the nano fraction volume parameter c on the tangential, circumferential velocity and temperature for both stable and unstable profiles respectively. There is a decline in the unstable velocity profiles along tangential direction and the unstable temperature profiles as the term (ϕ) magnifies, but the opposite trend is observed in stable and realisable solutions. Therefore, both the hydrodynamic and thermal boundary layer broaden with a rise in (ϕ) as found in Figures 2, 3 and 4.

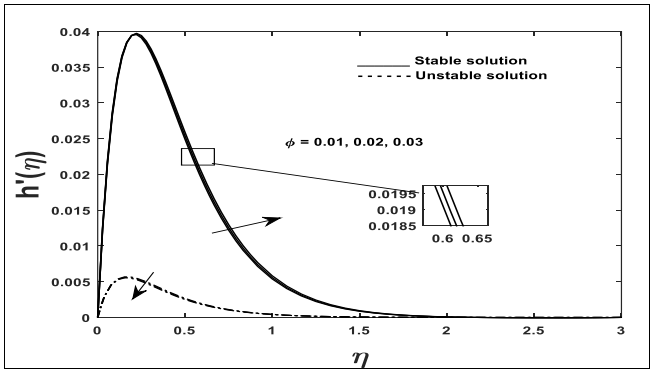

Fig 2: Variation of nano fractional values parameter (ϕ) with tangential velocity

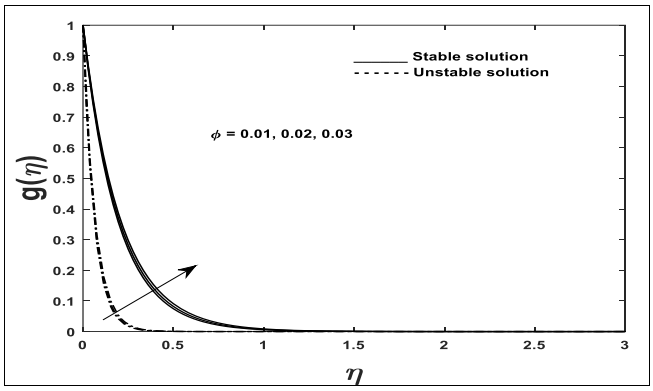

Fig 3: Variation of nano fractional values parameter (ϕ) with circumferential velocity

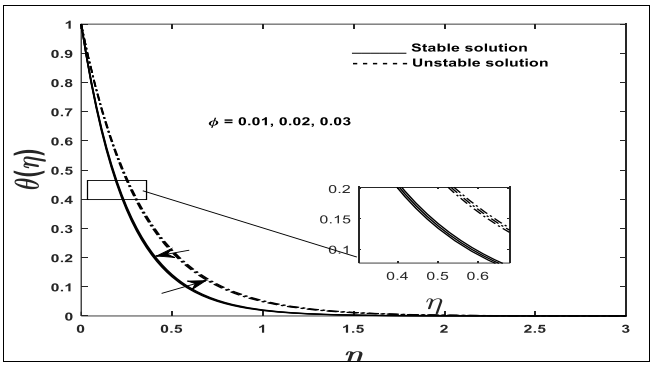

Fig 4: Variation of nano fractional values parameter (ϕ) with temperature

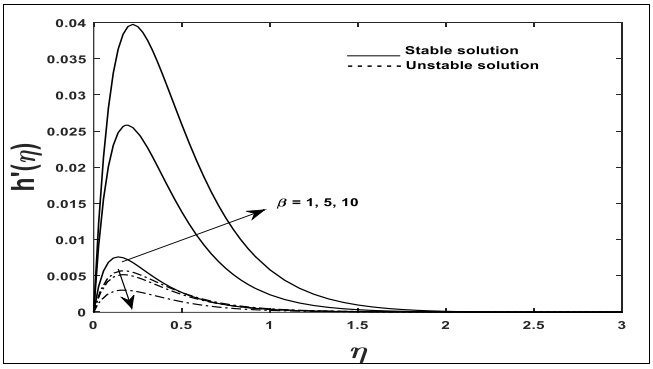

Fig 5: Variation of Casson fluid parameter (β) with tangential velocity

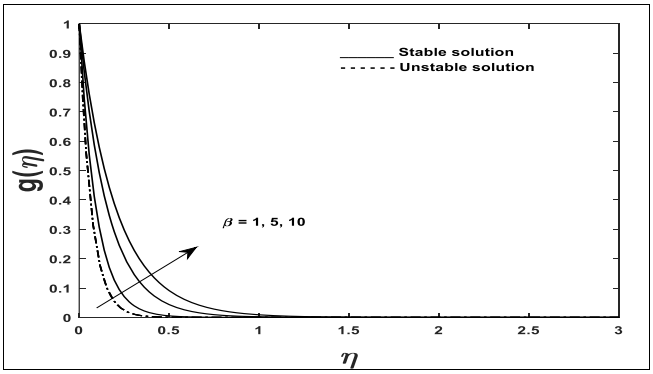

Fig 6: Variation of Casson fluid parameter (β) with circumferential velocity

It can be reaffirmed from the studies reported and the governing equations that, a rise in the Casson parameter often introduces additional burden on momentum equations due to its viscosity. As a result, there is a damping effects which as result increase the magnitude of both tangential and circumferential velocities of stable solutions and temperature profiles. These trends conform to physical intuition that increase in Casson parameter enhances the fluid particles and rapidly change the systems to allow fluid momentum and thermal boundary layers to propagate through the medium. As the Casson parameter (β) increases, the temperature profiles relatively amplified, indicating increase in heat propagation from the fluid surface into the interior. This trend is occasioned by a rise in fluid transport in both tangential and circumferential directions. The situation concord with what has been reported in Figure 5, 6 and 7. Translational and rotational effects of porosity parameter (ε) is depicted in Figure 8 and 9, it is reported enhanced porosity management increase retention of fluid particles at the surface of a plate, thereby thicken the momentum boundary layer which allow more fluid to flow.

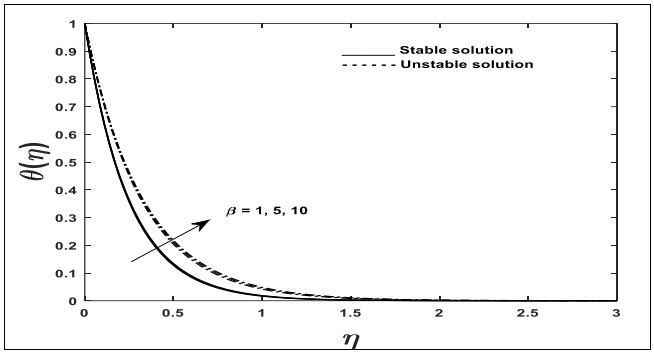

Fig 7: Variation of Casson fluid parameter (β) with temperature

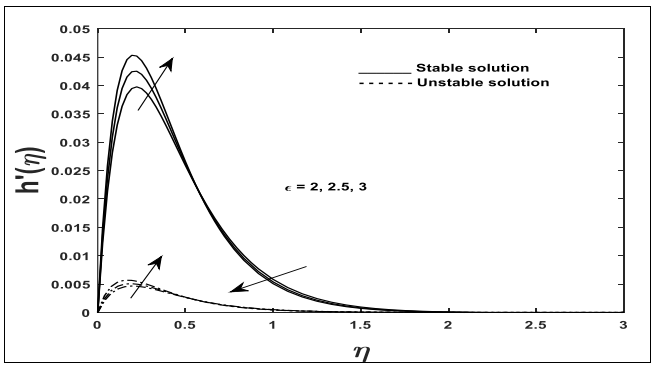

Fig 8: Variation of porousity parameter (ε) with tangential velocity

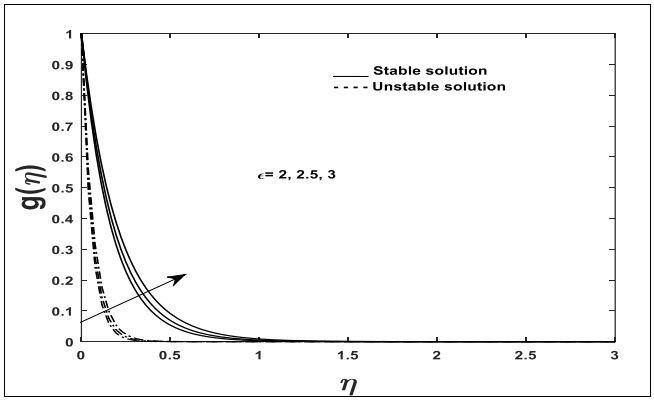

Fig 9: Variation of porosity parameter (ε) with circumferential velocity

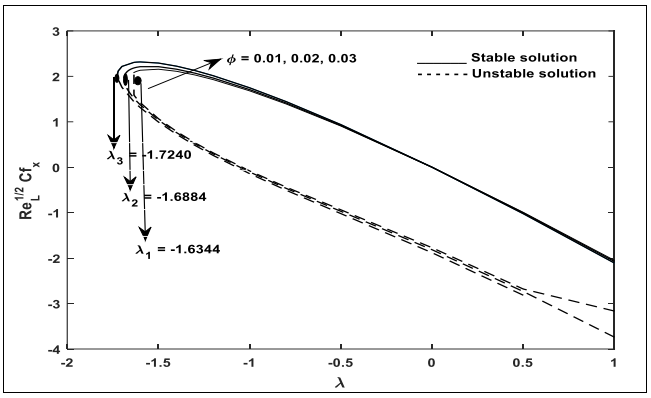

Fig 10: Effects of nano fraction parameter (ϕ) on $^{2^{-1}}\mathrm{Re}_L^{1/2} C_{fx}$

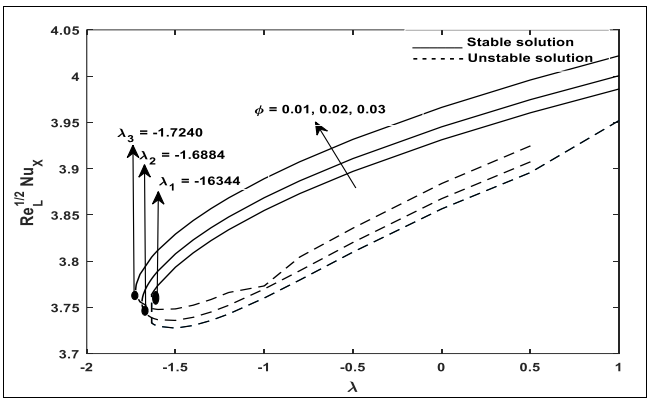

Fig 11: Effects of nano fraction parameter (ϕ) on $\mathrm{Re}_L^{1/2} Nu_x$

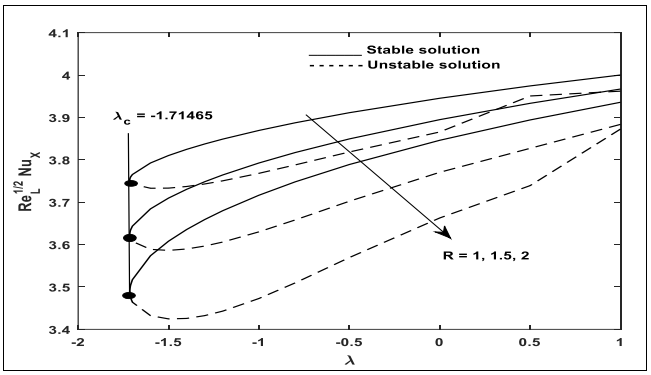

Fig 12: Effects of thermal radiation parameter (R) on $\mathrm{Re}_L^{1/2} Nu_x$

The effects of skin friction coefficient $Re_x^{1/2} C_f$ on velocity at the tangential direction against parameter λ as depicted in figure 11. Bifurcation of boundary layer attainment at opposing flow region and instability decays at a region where (λ= -1.7240), (λ = -1.6884) and (λ = -1.6344) in the first solution and the trend changes gradually toward aiding flow at (λ > 0). Demonstrated in figure 12 is the rate of heat transfer $\mathrm{Re}_L^{1/2} Nu_x$ against nano volume fraction parameter (ϕ). Rate of heat transfer invrease with increase in nano volume fraction parameter and bifurcation points remains unaltered.

An increase in radiation parameter R leads to upsurge in rate of heat transfer $Re_x^{-1/2} N u_x$. Bifurcation point remain constant (λ = -1.71465) when R = 1.0, 1.5, 2.0, this is demonstrated in figure 12. Physically it means that the heat generated by R caused the local Nusselt number $Re_x^{-1/2} N u_x$ increased and bifurcation remains in shrinking region (λ< 0).

4. Conclusion

The similarity transformations are used on governing partial differential equations of momentum and energy, which were converted into non dimensional ordinary differential equations and solve numerically using MATLAB bvp4c solver. The following conclusion is arrived with after numerical analysis of the results;

1. There is on the opposing flow a critical value *λc* below which no real or unique solutions exist. The critical value *jλcj* remains static with increase in thermal radiation parameter whereas it increases with increase in Cu-H2O nanoparticle volume fraction.
2. Stability analysis provided the smallest eigenvalue γ, which revealed that only the first solution is stable and physically realizable, whereas the second solution is unstable and unrealistic.
3. It is noticed that increase in radiative parameter attracts increase in temperature of the fluid at the opposing flow region.
4. The velocity of the fluid is appreciated with increase in copper volume fraction (ϕ) and depreciates with increase in velocity slip parameter (P).

5. Acknowledgement

The authors profoundly acknowledged the support received from Tertiary Education Trust Fund (TETFund), through Kebbi State Polytechnic Dakingari (Nigeria) for funding the research under Institutional Based Research (IBR).

6. Conflict of Interest

All the authors declared that no competing interest in this research.

7. References

1. Duguma KA, Makinde OD, Enyandene LG. Dual solution and stability analysis of Cu-HO2-Casson nanofuid convection past a heated stretching/shrinking slippery sheet in a porous medium. Computational Mathematical Methods. 2023, Article ID 6671523, 20 pages. Doi: https://doi.org/10.1155/2023/6671523
2. Animasaun IL. Effects of thermophoresis, variable viscosity and thermal conductivity on a free convective heat and mass transfer of non-Darcian MHD dissipative Casson fluid flow with suction and nth order chemical reaction. Journal of the Nigerian Mathematical Society. 2015; 34(1):11-31.
3. Aghamajidi M, Yazid ME, Dinavand S, Pop I. Tiwari-Das nanofluid model for Magnetohydrodynamic (MHD) natural convective fluid flow of a nanofluid adjacent to a spinning dawn-pointed vertical cone. Propulsion and Power Research. 2018; 7(8):78-90.
4. Hassan MM, Karim ME. Chemical reactive unsteady flow of Casson fluid over a stretching surface. Malaysian Journal of Science and Advanced Technology. 2025; 5(2):132-139.
5. Hayat T, Sahzad SA, Alsaedi A. Soret and Dufour effects on magnetohyrodynamic (MHD) flow of Casson fluid. Appl. Math. Mech, Engl. Edu. 2012; 33(10):1301-1312. Doi 10.1007/s10483-012-1623-6
6. Abideen ZU, Saif RS. Impact of thermal radiation and natural heat generation on Casson nanofluid flow by a curved stretchable surface with suspension of carbon nanotubes (CNTs). Heliyon. 2023; 9:e18941. Doi:

https://doi.org/10.1016/j.heliyon.2023.e18941
7. Gopal D, Kishan N. Brownian motion and thermophoresis effects on Casson nanofluid over a chemically reacting stretching sheet with inclined magnetic field. Appl. Appl. Math; An International Journal. 2018; 4:106-116.
8. Walelign T. Analysis of Casson nanofluid transport rates near a vertical stretching cheet with dissipation ans slip effects. Front; Appl. Math. Stat. 2025; 11:1526769. Doi: 10.3389/fams2025.1526769
9. Noranuor WN, Mohamad AQ, Jiann LY, Shafie S, Jamaludin MA. Analytical solution for MHD Casson nanofluid flow and heat transfer due to stretching sheet in porous medium. Journal of Advanced Research in Numerical Heat Transfer. 2024; 19(1):43-59. Doi: https://doi.org/10.37934/amht.19.1.4359
10. Pamigrahi L, Pands J, Swain K, Dash DC. Heat ans mass transfer of MHD Casson nanofluid flow through a porous medium past s stretching sheet with Newtonian heating and chemical reaction. Karbala Int. Journal of Modern Science. 2020; 6(3), Art. 11. Doi: https://doi.org/10.33640/2405-609X.1740
11. Narender G, Govardhan K, Sarma GS. MHD Casson nanofluid past a stretching sheet with effects of viscous dissipation, chemical reaction and heat source/sink. Journal Appl. Computer Mech. 2019; 7(4):2040-2048. Doi: 10.22055/JACM.2019.14804
12. Merkin JH. On dual solutions occurring in mixed convection in a porous medium. Journal of Engineering Mathematics. 1986; 20(2):171-179.
13. Oyolakin IS, Ghosh R, Modal S, Sibanda P. Entrophy generation in Casson nanofluid flow past an electromagnetic stretching riga plate. Malaysian Journal of Mathematical Sciences. 2021; 15(3):425-445.
14. Nabajyoti D, Sharma BR. Unsteady Free Convective Flow Pasta Vertical Cone in the Presence of Chemical Reaction and Thermal Radiation Effects. International Journal of Applied Engineering Research. 2019; 14(5):1084-1090.
15. Saleem S, Hunza R, Al-Qahtani A, Abd-El-Aziz M, Malik MY, Animasaun IL. Magneto Jeffrey NonafluidBioconvection over a Rotating Vertical Cone due to Gyrotatic Microorganism. Mathematical problems in Engineering. Hindawi, Art. ID 3478037, 2019, p. 11.
16. Sharma BK, Konwar H. MHD flow, heat and mass transfer about a permeable rotating vertical cone in the presence of radiation, chemical reaction and heat generation/ absorption effects. Latin America Applied Research. 2019; 46:109-114.
17. Salem S. Heat and mass transfer of rotational flow of third grade fluid over a ratoating cone with buoyancy effects. Mathematical Probems in Engineering, Art. I.D. 5544540, 2021, p. 9. Doi: https://doi.org/10.1155/2021/5544540
18. Huang CJ, Yih KA. Non-linear radiation and variable viscosity effects on free convection of a power-law nanofluid over a truncated cone in porous media with zero nanoparticles flux and internal heat generation. Journal of Thermal Science Engineering Application. 2021; 13(3):031020 (11 pages)
19. Wahid NS, Arifin NM, Kashi'ie NS, Pop I, Bachok N, Hafidzuddin ME. Mixed convective magnetic nanofluid flow past a rotating vertical porous cone. Journal of Applied Fluid Mechanics. 2022; 15(4):1207-1220.
20. Ahmad S, Ali K, Bashir H. Interaction of Micropolar Fluid Structure with the Porous Media in the Flow due to Rotating Cone. Alexndria Engineering Journal. 2021; 60:1249-1257.
21. Ganesh NV, Hakeem AKA, Ganga B. Darcy-Forchheimer hydromagnetic nanofluid over a stretching/shrinking sheet in a thermally stratified porous medium with second order slip, viscous and ohmic dissipation effects. Aim Shams Engineering Journal, 2016. Doi: https://doi.org/10.1016/j.asej.2016.04.017
22. Muhammad J, Hameed MK, Nisar KS, Majeed AH. Darcy-ForchheimerFlow of MaxwellNanofluid flow over a porous stretching sheet with Arrhenius activation energy and field boundary conditions. Case Study in Thermal Engineering. 2023; 44:102830. Doi: https://doi.org/10.1016/j.csite 2023.102830
23. Upreti H, Pandey AK, Kumar M, Makinde OD. Ohmic heating and a non-uniform source/sink roles on 3D Darcy-Forchheimer flow of CNTs nanofluid over a stretching surface. Arab Journal of Science Engineering. 2020; 45:7705-7717.
24. Loganathan K, Nazek A, Fehaid A, Salem A. Significances of Darcy-Forchheimer porous medium in third grade Nanafluid with entropy features. European Physical Journal Special Topics. 2021; 230:1293-1305.
25. Chunyan L, Khan MS, Ramza M, Chu MY, Kadry S, Malik MY, Charam R. Non-linear radiative Maxwell nanofluid flow in a Darcy-Forchheimer permeable media over a stretching cylinder with chemical reaction and biconvection. Scientific Report. 2021; 11(1):9391. Doi: https://doi.org/10.1038/s41598-021-88947-5
26. Verma K, Debozani B, Sharna B. Soret and Dufour effects on MHD flow about a rotating vertical cone in the presence of radiation. Engineering Physics; Journal of Mathematical and Computational Science. 2021; 11(2):3188-3204.